iScience

CellPress
OPEN ACCESS

Article

# Spatial definition of the human progesterone receptor-B transcriptional complex

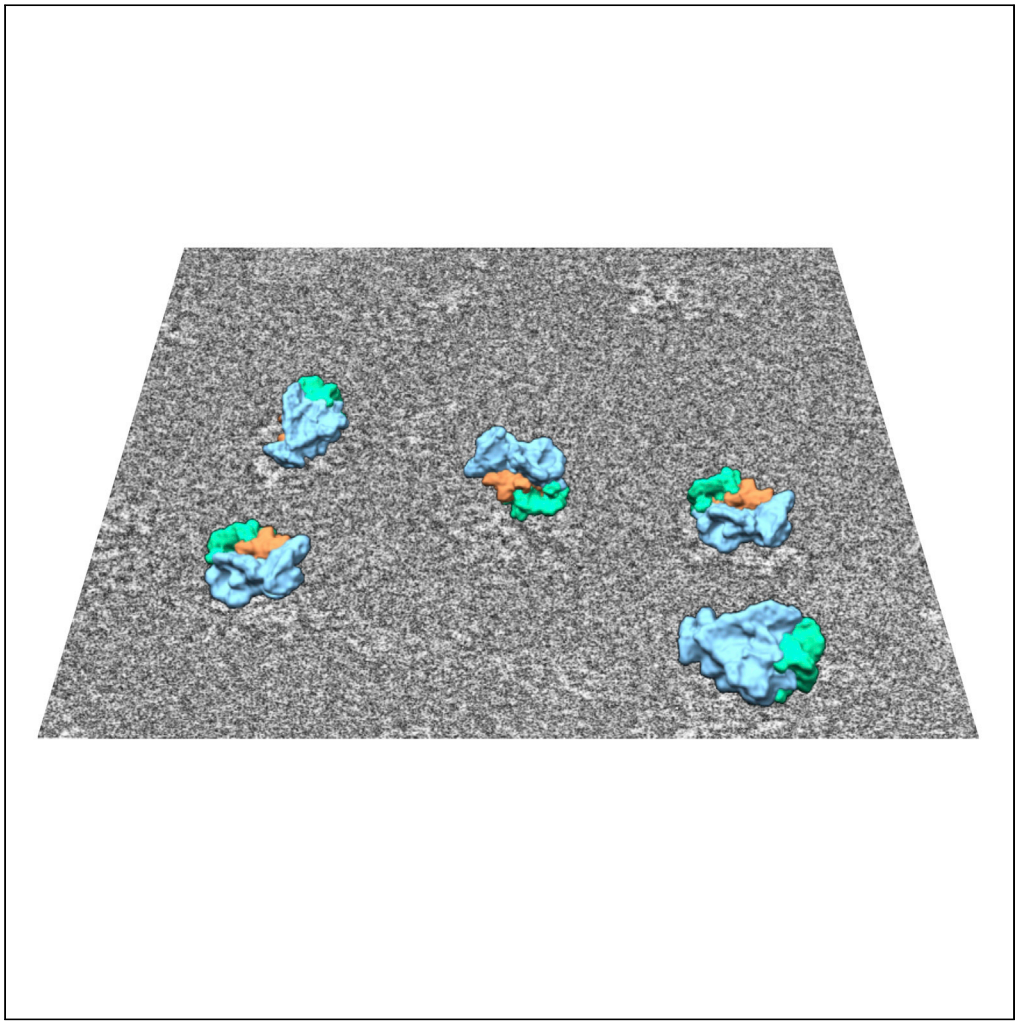

Xinzhe Yu, Ping Yi, Anil K. Panigrahi, ..., Steven J. Lutdke, Zhao Wang, Bert W. O'Malley

zhaow@bcm.edu (Z.W.)
berto@bcm.edu (B.W.O.)

## Highlights

Structure of the transcriptional complex for the full-length progesterone receptor-B

Contributions of AFs in forming the PR-B dimer interface and PR-B/coactivator complex

Unique mechanism of PR-B complex different from two other steroid receptor complexes

Yu et al., iScience *25*, 105321
November 18, 2022 
https://doi.org/10.1016/j.isci.2022.105321

iScience

CellPress
OPEN ACCESS

Article

# Spatial definition of the human progesterone receptor-B transcriptional complex

Xinzhe Yu,[1,2,6] Ping Yi,[1,4,5,6] Anil K. Panigrahi,[1] Lance Edward V. Lumahan,[1] John P. Lydon,[1] David M. Lonard,[1] Steven J. Lutdke,[2,3] Zhao Wang,[1,2,3,4,*] and Bert W. O'Malley[1,4,7,*]

## SUMMARY

**We report the quaternary structure of core transcriptional complex for the full-length human progesterone receptor-B (PR-B) homodimer with primary coactivator steroid receptor coactivator-2 (SRC-2) and the secondary coactivator p300/CREB-binding protein (CBP). The PR-B homodimer engages one SRC-2 mainly through its activation function 1 (AF1) in N-terminus. SRC-2 is positioned between PR-B and p300 leaving space for direct interaction between PR-B and p300 through PR-B's C-terminal AF2 and its unique AF3. Direct AF3/p300 interaction provides long-desired structural insights into the known functional differences between PR-B and the PR-A isoform lacking AF3. We reveal the contributions of each AF and demonstrate their structural basis in forming the PR-B dimer interface and PR-B/coactivator complex. Comparison of the PR-B/coactivator complex with other steroid receptor (estrogen receptor and androgen receptor) complexes also shows that each receptor has its unique mechanism for recruiting coactivators due to the highly variable N-termini among receptors.**

## INTRODUCTION

As the apex hormone of pregnancy, progesterone is indispensable for female fertility and overall reproductive health (DeMayo and Lydon, 2020). Along with infertility and early pregnancy loss, dysregulation of the progesterone response promotes myriad pathologies, from endometriosis and leiomyoma to endometrial and mammary gland tumorigenesis (Diep et al., 2015; Horwitz and Sartorius, 2020; Ishikawa et al., 2010; Kim et al., 2020; Patel et al., 2015). The majority of these cellular and tissue responses to progesterone are mediated by the progesterone receptor (PR).

The PR is a key member of the nuclear receptor (NR) superfamily of transcription factors (O'Malley, 2020; Tsai and O'Malley, 1994), which also includes the estrogen and androgen receptors (ERα and AR, respectively). With ERα and AR, PR completes the triad of NRs for sex steroid hormones that control female and male reproductive biology. The PR is a multidomain allosteric transcription factor that shares with NR family members a common functional domain organization, which includes an N-terminal domain (NTD), a centrally located DNA-binding domain (DBD) with a hinge region, followed by a ligand-binding domain (LBD) at the C-terminus (Grimm et al., 2016).

Like other NR superfamily members, PR contains two activation function (AF) domains: AF1 and AF2 (Grimm et al., 2016). Located within the NTD, the ligand-independent AF1 domain is intrinsically disordered, modular, and lacks evolutionary conservation with other NR members. Mapped to the LBD, the ligand-dependent AF2 is significantly more conserved to other NR members and is highly structured. Early biochemical studies on PR indicated that additional steroid receptor coactivator (SRC) interaction surfaces reside within the PR NTD, of which only a portion maps to the AF1 (Onate et al., 1998). Although lacking structural support at the time, these findings suggested that optimum NR transcriptional activity requires functional synergy between AF domains (Tetel et al., 1999).

Unique to the NR superfamily, the PR exists naturally as two functionally distinct receptor isoforms (PR-A and PR-B), which are identical to each other except that the PR-A isoform lacks the first 164 amino acids (aa) present in the N-terminus of PR-B (Dong et al., 2004; Sartorius et al., 1994; Tung et al., 2001, 2006). While both PR isoforms possess AF1 and AF2 domains, the PR-B isoform contains a context-dependent AF3 domain, which is located within the N-terminal 164 aa sequence. Early cell-based reporter assays

[1]Department of Molecular and Cellular Biology, Baylor College of Medicine, Houston, TX 77030, USA

[2]Verna and Marrs McLean Department of Biochemistry and Molecular Biology, Baylor College of Medicine, Houston, TX 77030, USA

[3]CryoEM/ET Core, Baylor College of Medicine, Houston, TX 77030, USA

[4]Dan L Duncan Comprehensive Cancer Center, Baylor College of Medicine, Houston, TX 77030, USA

[5]Center for Nuclear Receptor and Cell Signaling, Department of Biology and Biochemistry, University of Houston, Houston, TX 77204, USA

[6]These authors contributed equally

[7]Lead Contact

*Correspondence: zhaow@bcm.edu (Z.W.), berto@bcm.edu (B.W.O.)

https://doi.org/10.1016/j.isci.2022.105321

suggested that the AF3 domain contributes in part to promoter-specific transactivation differences between the two isoforms (Takimoto et al., 2003); however, it remains unclear how the addition of AF3 regulates PR transcriptional activity.

DNA-bound NRs—through a sequential and processive recruitment process—interact with members of the SRC/p160 family of primary coactivators, which in turn recruit secondary coactivators (i.e. p300/CREB-binding protein [CBP]) to form their respective core coregulator transcriptional complexes (O'Malley, 2003). Our previous cryo-EM structural studies demonstrated that ERα and AR utilize different functional domains to recruit coactivators, and their highly variable NTDs support formation of the dimerization interface and are key determinants of receptor-coactivator interaction mechanisms (Yi et al., 2021; Yu et al., 2020). Compared to ERα, AR has a longer NTD that surrounds the LBD to mask the LBD-coactivator interaction surface, resulting in a stronger AF1 function. PR-B has an NTD that is comparable with AR in length. In contrast to AR, the AF2 of PR is a potent transcriptional activator (Meyer et al., 1990) but the underlying reason for its differential activation function is not well understood.

Structural insights that define the stoichiometry and topological arrangement of the individual components of DNA-bound NR core coactivator transcriptional complexes have been valuable for gaining fundamental insights into their control of gene expression (Yi et al., 2021). Here, we present structures of a DNA-bound PR-B dimer and a PR-B/SRC-2/p300 core complex by single-particle cryo-EM, further validated through functional interaction experiments. Our studies demonstrate that PR-B adopts a distinct dimerization and coactivator assembly architecture compared to ERα and AR. Thus, structural analyses reveal that ERα, AR, and PR-B utilize distinct conformations to recruit coactivators and activate transcription despite having a similar, modular arrangement of their AF1, DBD, and LBD/AF2 domains.

## RESULTS

### The three-dimensional structure of the liganded full-length PR-B homodimer bound to DNA

The transcriptional activity of recombinant human PR-B protein, which was purified from baculovirus, was tested using an *in vitro* transcription assay using a chromatinized growth regulating estrogen receptor binding-1 (GREB1) composite DNA template (Panigrahi et al., 2018). The GREB1 composite fragment was constructed using GREB1 enhancer and promoter regions that contain progesterone response elements (PREs). Addition of increasing concentrations of purified recombinant PR-B protein in the presence of progesterone gradually increased the levels of *in vitro*-transcribed *GREB1* mRNA (Figure S1A), confirming that the purified PR-B protein is functionally active. For single-particle cryo-EM experiments, recombinant PR-B protein was incubated with a short PRE oligonucleotide (32 bp) in the presence of progesterone. The liganded DNA-bound PR-B sample was directly applied to cryo-EM grids and subjected to standard single-particle cryo-EM data collection and analyses (see STAR Methods section). Representative raw images of DNA-bound PR-B are shown in Figure S1B. We resolved a structure at ~11 Å resolution (Figures 1A and S1C) based on the gold standard Fourier shell correlation (FSC) (Henderson et al., 2012). In the presence of progesterone, PR-B forms a homodimeric structure that binds to DNA. Similar to our previous DNA-bound AR dimer structure (Yu et al., 2020), the DNA-bound PR-B dimer map contains a DNA-like density that defines the location of PRE-DNA bound by the two DBDs (Figure 1B). The reconstructed structure presents a pseudo 2-fold symmetry reflecting formation of a dimer. Following a similar segmentation procedure reported for complexes of DNA-bound liganded ERα and AR (Yi et al., 2015; Yu et al., 2020), we performed segmentation on the reconstructed PR-B map and assigned densities using a combination of relative molecular mass, known binding domains, and antibody-binding results (Figures 1B and S2). The NTD density map was further segmented into subregions (AF1, AF3, and the rest of the NTD located between the AF1 and AF3 labeled as rNTD). To confirm the assignment of AF3, we incubated the PRE/PR-B sample with a PR-B-specific antibody fragment (N-Fab) which recognizes the 164 aa N-terminal extremity that is present in PR-B but not in PR-A. The reconstructed Fab-bound PRE/PR-B structure is similar to the PRE/PR-B structure with the exception of two protruding densities indicating the binding of an N-Fab to each PR-B monomer (Figures S2A and S2B). The two N-Fab densities are restricted to the AF3 region in the segmented density map, thereby confirming the AF3 annotation. We assigned the region connecting AF1 and AF3 as rNTD-a and rNTD-b for each PR-B-monomer. Furthermore, we labeled the LBD using another Fab fragment (C-Fab) generated from an antibody that selectively recognizes the C-terminal end of PR-B (919-933aa), next to the AF2 region (904-919aa) (Danielian et al., 1992). As shown in Figures S2C and S2D, two C-Fabs bind to the region assigned as the LBD in the segmented map and are positioned at the interaction interface between the LBD and the AF3. This result is consistent with

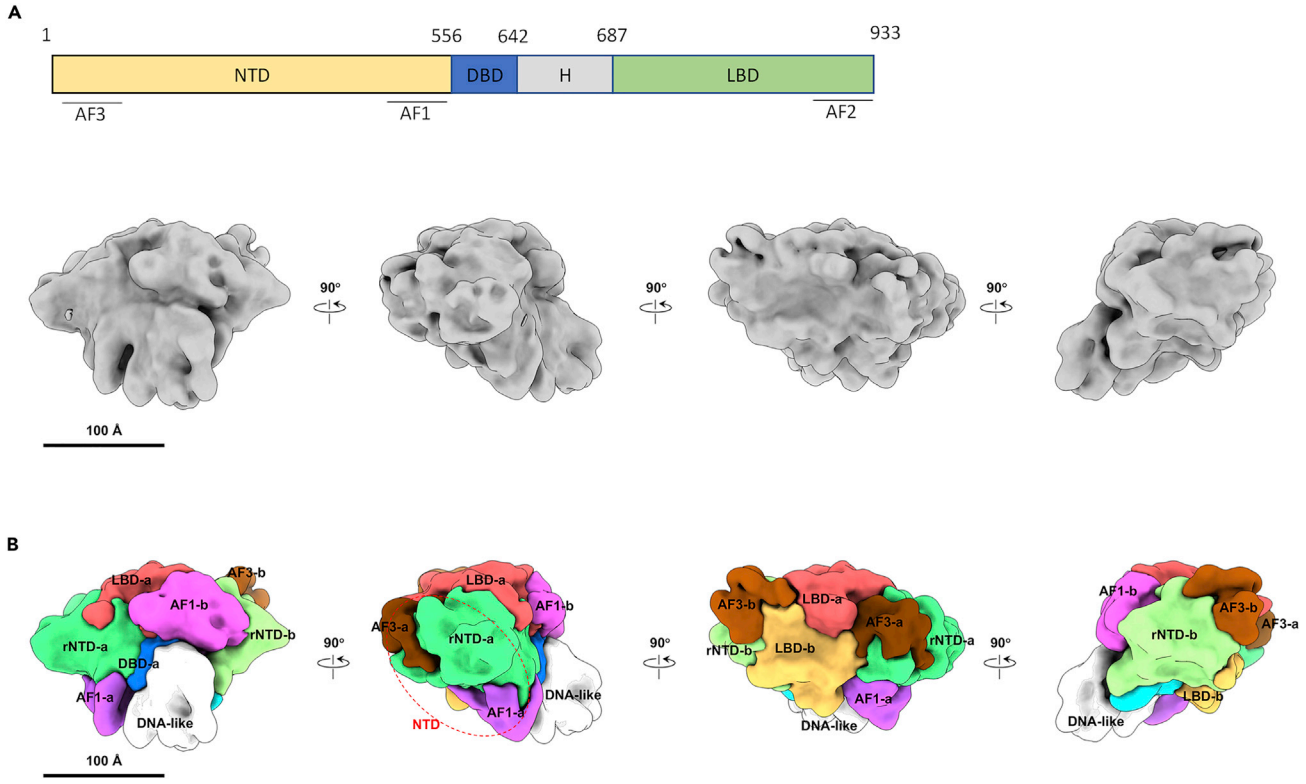


**Figure 1. Density map and segmentation of DNA-bound liganded PR-B dimer**

(A) Cryo-EM map of PRE-DNA/PR-B at a resolution ~10.9 Å viewed from different orientations.

(B) Segmentation of PRE-DNA/PR-B. The segments of two PR-Bs are shown as -a and -b separately. The functional domains of PR-B are annotated in different colors. The NTD (dash circled) contains AF3 (Brown and light Brown), AF1 (Purple and light Purple), and the rNTD (the NTD region located between the AF1 and AF3 colored in Green and light Green). LBD: ligand binding domain (Orange and Red); DBD: DNA binding domain (Blue and light Blue). A DNA-like feature is colored in White. See also Figures S1 and S2 and Table S1. The scale bars represent 100 angstrom.

an earlier finding that the 30-aa C-terminal end of the PR-B isoform is essential for contact between the LBD and the AF3 (Dong et al., 2004). Collectively, the above antibody-labeling results confirm our PR-B dimer domain segmentation analyses.

The DNA-bound PR-B dimer structure reveals that the two LBD densities are in the middle of the dimerization interface with the two NTDs located on each side of the LBDs. However, the two NTDs do not come into strong contact with each other. This NTD-LBD organization is strikingly different from our previously reported AR dimer structure (Yu et al., 2020) (Figure 2) in which the AR NTDs wrap around the LBDs before contacting each other, essentially encasing the LBDs. On the other hand, the ERα dimer density from the ERα/SRC-3/p300 complex map is comparable to the PR-B dimer density except that ERα contains a significantly shorter NTD (Figure 2). Although the structure of the PR-B LBD dimer is similar to the AR LBD dimer, the PR-B LBD adopts a different orientation toward the DNA and DBD (Figure S4). Comparison of these three steroid receptor dimer structures demonstrates that they do not adopt the same dimerization mechanisms despite having similar domain organization.

## Quaternary structure of the DNA-bound PR-B/SRC-2/p300 core transcriptional complex

We previously demonstrated that AR recruits primary and secondary coactivators through its NTD while ERα recruits two SRC-3 through its LBD (Yi et al., 2021). Here, we examined how PR-B recruits core coactivators. Because of its importance in a number of progesterone-dependent physiological processes (Kommagani et al., 2013, 2014; Mukherjee et al., 2006), SRC-2 was chosen as the primary coactivator in these structural studies. In our *in vitro* transcription assay, we found that immunodepleting SRC-2 and p300 abolished PR-B-mediated *GREB1* transcription (Figure 3A), demonstrating that SRC-2 and p300 are essential primary and secondary coactivators, respectively, for affecting PR-B-mediated transactivation. Adding

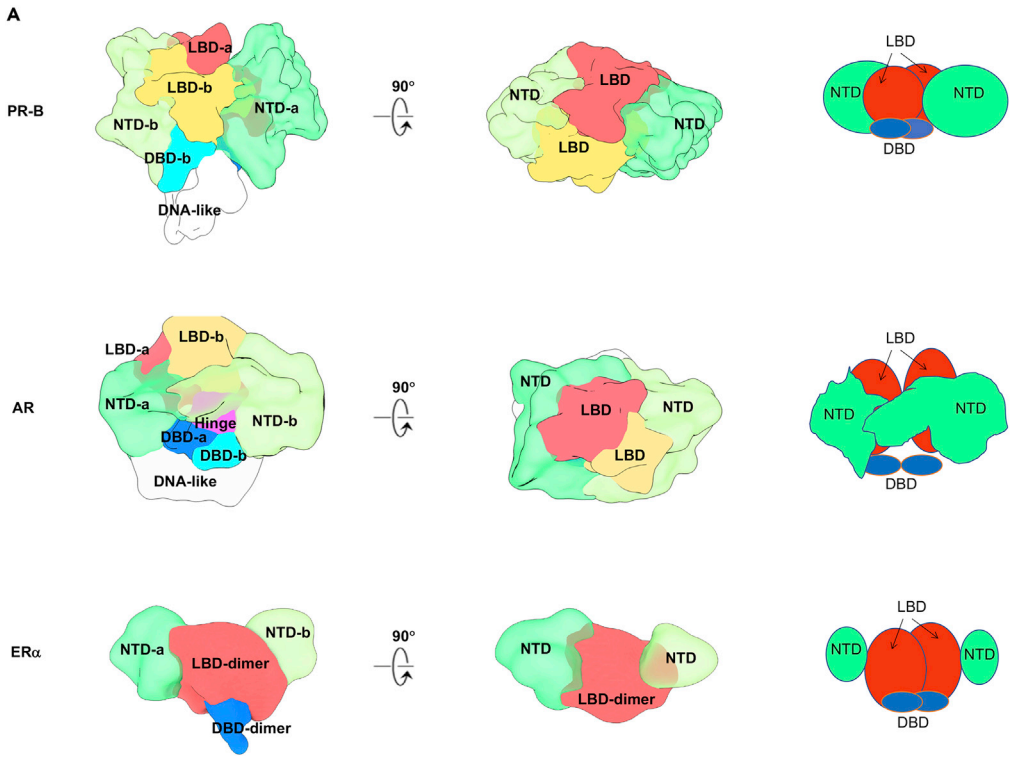


**Figure 2. Structural comparison of the PR-B, AR, and ERα dimers on DNA**

PR-B, AR, and ERα densities in two different views show different arrangements of the LBD and NTD. PR-B and AR are segmented DNA bound dimer density while ERα is extracted from ERE-DNA/ERα/p300/SRC-3 complex. The cartoon illustrations of the three receptors are shown at the right. All three densities show LBD in the center. The NTDs of PR-B and ERα are packed at two sides of the LBDs while the LBDs of AR are encircled by its large NTDs. See also Figure S4.

back both purified recombinant SRC-2 and p300 (but not each individually) largely restored PR-B-mediated transcriptional activity (Figure 3A). This result confirms that our purified recombinant SRC-2 and p300 are functionally active. The assembly of the DNA-bound PR-B/SRC-2/p300 complex was accomplished by incubating the three purified recombinant proteins with progesterone and biotinylated PRE-DNA, followed by DNA pull-down with streptavidin beads and the enzymatic release of the complexes from the beads (Yi et al., 2015, 2017; Yu et al., 2020). Following a standard single-particle cryo-EM pipeline, we collected raw images of the complex as shown in Figure S1D. Using RELION (Punjani et al., 2017; Scheres, 2012), we resolved a density map of the PRE-DNA-bound PR-B/SRC-2/p300 complex (Figure 3B). The complex density map has a dimension of ~160 x 220 x 240 Å with a resolution of ~19 Å based on FSC (Figure S1E) (Henderson et al., 2012). The density map was then segmented, and each component was identified (Figure 3B). Our results indicate that the PR-B dimer recruits only one SRC-2 and one p300, which resembles the AR-coactivator complex but not the ERα-coactivator complex (Yi et al., 2015; Yu et al., 2020) (Figure S4). However, the overall shape of the complexed SRC-2 resembles the SRC-3 densities in the AR and ERα transcriptional complexes. The p300 density is also similar to the p300 density in the ERα-coactivator complex or the free antibody-labeled p300 structure (Yi et al., 2015). Alignment of these p300 structures indicates that the SRC-interaction domain (SRCID) at the C-terminal end of p300 is positioned at the p300-SRC-2 interaction interface (Figure S5), confirming previous reports that the SRCID is necessary for p300-SRC interaction (Kamei et al., 1996). Next, we docked the segmented PRE-DNA/PR-B structure into the PR-B density within the complex (Figures 3D and S6) to understand how each domain of PR-B is engaged in coactivator binding. To ensure correct docking, we labeled the DNA-bound PR-B/SRC-2/p300 complex with a PR-B N-Fab antibody (Figures S3A and S3B). Aligning the position of the N-Fab antibody in the complex map with its position in the segmented PR-B dimer map further guided the replacement. As shown in Figure 3C, p300 has multiple contacts with the NTD and LBD of PR-B. The AF3 is the primary region of the NTD that interacts with p300. We found that the C-Fab-labeled region (Figure S2D), which is adjacent to the AF2-a, is located at the p300 docking site, suggesting that the AF2 also contributes to the interaction

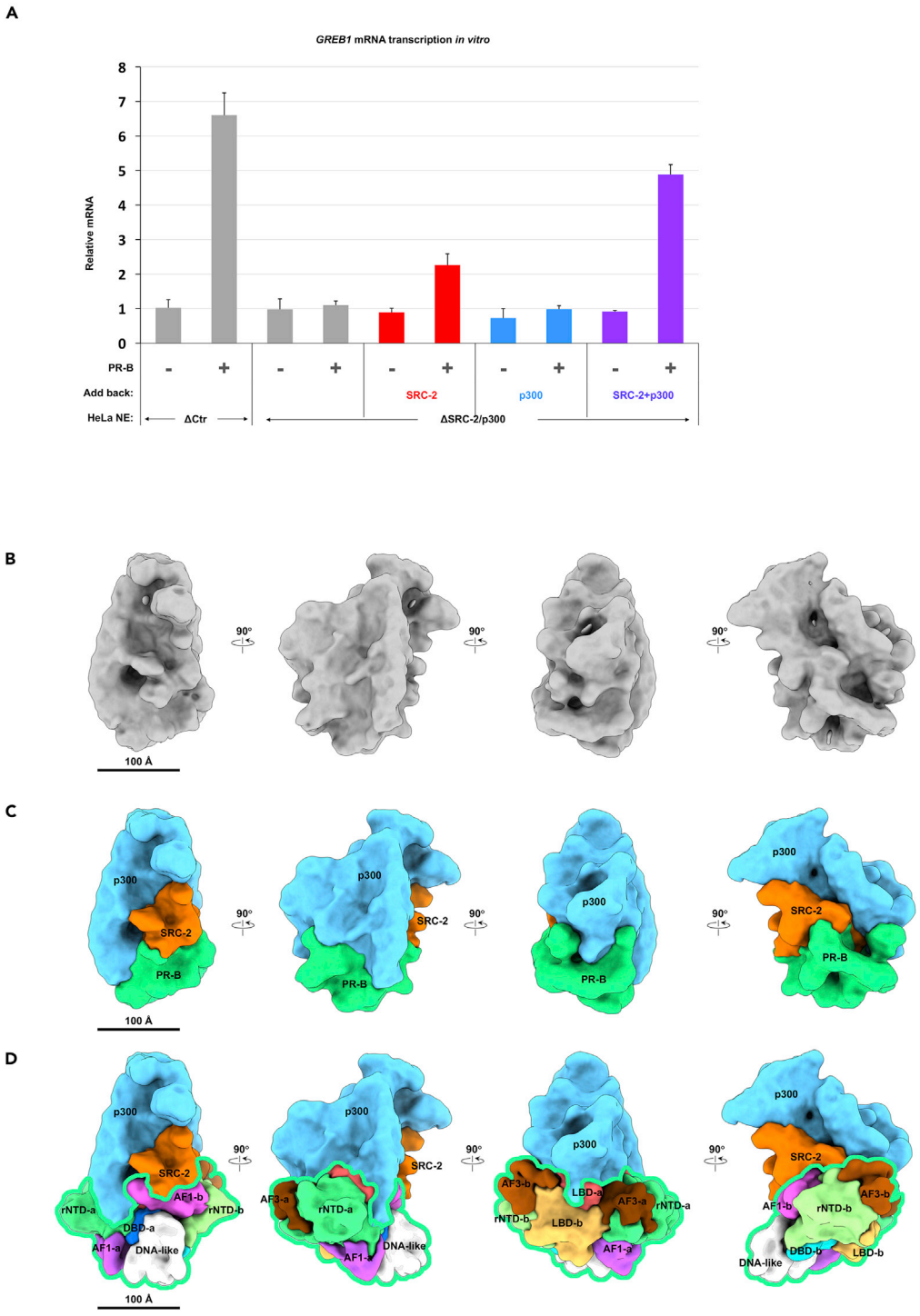


**Figure 3. The structure of PRE-DNA-bound PR-B/SRC-2/p300 complex**

(A) Purified recombinant PR-B, SRC-2, and p300 proteins activate PR-targeted gene transcription *in vitro*. Chromatinized PR-targeted gene *GREB1* composite template with endogenous enhancer and promoter elements (CompF template) was transcribed *in vitro* with HeLa nuclear extract (NE) after control immunodepletion (ΔCtr) and immunodepletion of both SRC-2 and p300 (ΔSRC-2/p300). Reactions were then supplemented with recombinant purified PR-B, SRC-2, and p300 as indicated. HeLa NE lacking SRC-2 and p300 fails to support PR-B-dependent transcription activation, which is rescued by addition of recombinant SRC-2 and p300 demonstrating that our purified PR-B, SRC-2, and p300 are functionally active. The error bars represent standard error of the mean.

**Figure 3. *Continued***
(B) Cryo-EM density map of the PRE-DNA-bound PR-B/SRC-2/p300 complex at 19.1 Å resolution. Shown are 4 different angles of the map rotating every 90 degrees.
(C) Segmentation of PRE-DNA/PR-B/SRC-2/p300. Each component was segmented to annotate different proteins: PR-B, Green; SRC-2, Orange; p300, Blue, respectively.
(D) The assembled PRE-DNA/PR-B/SRC-2/p300 structure with segmented PRE-DNA/PR-B density (Figure 1B) replacing the PR-B density. The green outline represents the replaced density from the PRE-DNA/PR-B complex. See also Figures S1, S3, S5, and S6 and Table S1. The scale bars represent 100 angstrom.

with p300. Together, the two AF3s and AF2-a form a docking site for p300 binding. A part of AF1 is also involved in interacting with p300. SRC-2 was shown to mainly interact with the AF1 region of the NTD with a modest interaction with the LBD-a. A close contact between SRC-2 and p300 within the complex was detected, which comprised a long interaction interface. Altogether, through multiple contacts between each other, the three proteins form a stable DNA-bound complex.

### Functional domain interactions between PR-B, SRC-2, and p300

We next examined the contributions of each PR-B functional domain in recruiting SRC-2 and p300 to confirm the cryo-EM structure. We generated three GST-fused PR-B fragments, AF1 (401–546 aa), AF3 (1–170 aa), and LBD (688–933 aa, which contains the AF2). These fragments were expressed in *E. coli.*, purified, and then incubated with purified recombinant full-length SRC-2 or p300 protein. Progesterone was added to the PR-B LBD fragment and SRC-2 or p300 mixture to facilitate ligand-dependent interaction. A GST pull-down experiment was then performed to examine PR-B fragments associated with SRC-2 or p300. As shown in Figure 4A, SRC-2 interacts strongly with the AF1 of PR-B. This is consistent with the cryo-EM structure of the PR-B/SRC-2/p300 complex where SRC-2 was observed to contact the AF1 region (Figure 3D). The p300 protein interacted with all three fragments of PR-B (Figure 4A), confirming our structural conclusions that p300 contacts both the NTD and LBD of PR-B within the core transcriptional complex (Figure 3D).

It is known that the LXXLL motifs present in the SRC receptor interaction domain (RID) interact with NR LBDs in a ligand-dependent manner. However, we observed that SRC-2 interacts with AF1, suggesting that a region other than the RID of SRC-2 may be involved in the interaction with the PR-B NTD. To test this, we generated five GST-fused SRC-2 fragments, corresponding to the bHLH/PAS (basic helix-loop-helix/Per-Arnt-Sim), S/T (Ser/Thr rich region), RID, CID (CBP/p300 interaction domain), and HAT (Histone acetyltransferase) domains (Figure 4B). A GST pull-down experiment was performed to examine the interaction between these fragments and purified PR-B. We found that the HAT domain interacts with PR-B in addition to the known RID interaction (Figure 4B), suggesting that the HAT domain is involved in the AF1 interaction.

There is a substantial contact surface between SRC-2 and p300 in addition to the p300-PR-B and SRC-2-PR-B interactions. Through the GST pull-down experiments, we demonstrate that several domains of SRC-2, including S/T and HAT, interact with p300 in addition to the known CID (Figure 4C). This result suggests that the two coactivators recruited by PR-B have strong connections with one another via multiple domain interactions, which help to enhance and sustain the complex integrity.

In summary, our cryo-EM and biochemical studies demonstrate the functional role of AF1 in recruiting SRC-2 and cooperative action of AF3 and AF2 in recruiting p300. Each of the protein components has tight contacts with the other two proteins within the complex to form a core functional active transcription unit (Figure 5). We also found that the three steroid receptors (PR-B, ERα, and AR) have different complex assembly mechanisms as summarized in Table 1.

## DISCUSSION

The AF3 domain not only distinguishes PR-B from other members of the NR superfamily but also has long been assumed to underpin the distinct transactivational properties that differentiate the PR-A and PR-B isoforms from each other (Sartorius et al., 1994; Tung et al., 2001, 2006). Using isolated functional domain fragments, biochemical studies have implicated AF3 as a major contributor to PR-B's tertiary structure; as an intramolecular interface for other regions of PR-B, including AF1, AF2, and the DBD; and as a key interacting surface for accessory proteins, such as nuclear coactivators. In the case of the AF2 containing LBD, early investigations demonstrated that the more conserved C-terminal region of NRs undergoes a

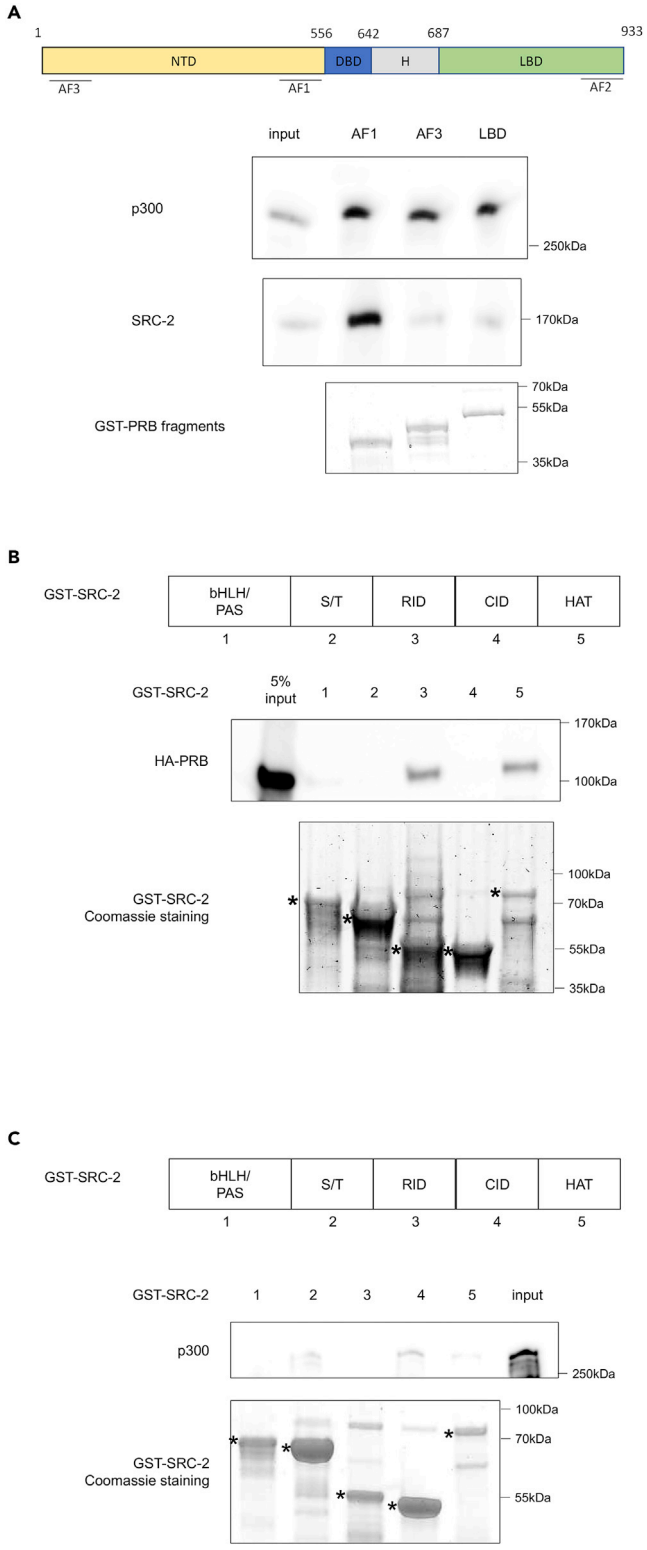


**Figure 4. Domain interactions between PR-B, SRC-2, and p300**

(A) The interaction between PR-B functional domains and SRC-2, p300. Upper and Middle panels are the Western blot results of GST-fused PR-B fragments-associated p300 or SRC-2 protein, respectively. The bottom panel is the Coomassie staining of PR-B fragments pulled-down using the glutathione beads.

**Figure 4. *Continued***
(B and C) The SRC-2 domains involved in interacting with PR-B (B) or p300 (C). GST-fused SRC-2 functional domains were incubated with purified PR-B or p300 protein followed by GST pull-down experiments. Shown are Western blot results of associated PR-B or p300. The positions of fragment bands on the coomassie staining are labeled by stars. See also Figures S1–S3 and S5.

ligand-dependent conformational change that results in formation of an AF2 hydrophobic pocket that docks with a RID containing LXXLL motif within primary SRCs (Hill et al., 2012). Mapped to an intrinsic disordered region just upstream of the DBD within the PR-B NTD, the ligand-independent AF1 has been implicated in the molecular recognition and assembly of primary coactivators (Goswami et al., 2014; Kumar et al., 2013; Onate et al., 1998; Wardell et al., 2005; Woo et al., 2019). While multiple biochemical investigations have uncovered important aspects of their transactivational roles, a structural framework for providing a mechanistic understanding of how these functions are integrated within the context of full-length PR-B assembled with full-length coactivators as an active and intact core transcriptional complex has been missing.

Here, we describe the cryo-EM structures of the DNA-bound full-length PR-B homodimer as well as its higher order assembly with full-length SRC-2 and p300. Our structural model indicates a 2-fold symmetrical structure in which the two PR-B LBDs (LBD-a and LBD-b) mediate a strong interaction between the PR-B monomers within the dimer's center. This finding agrees with previously published crystal structures that underscored the importance of both LBDs in PR-B dimerization (Williams and Sigler, 1998). Comprising nearly half of the PR-B protein, the intrinsically disordered NTD of each monomer closely associates not only with their corresponding LBDs but also with the LBD of their monomer partner. The structural consequences of this NTD-LBD association are close intermolecular positioning of the NTD-AF3a and NTD-AF3b with LBD-AF2b and LBD-AF2a, respectively. This spatial arrangement supports intermolecular "functional synergy" between AF3 and AF2 within the PR-B dimeric complex in addition to physically contributing to a tighter dimer. The exposed location of both AF3 regions along with interposed LBD regions demonstrates that a prominent interface surface exists for coactivator recruitment. The structure of the liganded PR-B dimeric complex bound to its target DNA element reveals both topological similarities and differences with the corresponding dimeric complexes for ERα and AR (Yi et al., 2015; Yu et al., 2020). While a similar spatial orientation is shared by the PR-B and ERα homodimers—LBDs in the center of the complex with flanking NTDs on the outside—the significantly longer PR-B NTD with its additional AF3 extremity leads to a different coactivator assembly mechanism for PR-B compared to ERα when forming their respective core transcriptional complexes. While PR-B and ERα adopt a tail-to-tail 2-fold symmetry on DNA, the AR monomers form a unique head-to-head and tail-to-tail arrangement (Yu et al., 2020), with their long NTDs encircling their LBDs. The AR NTD encirclement not only masks the AF2 containing LBD but also results in direct contact of the AR NTD at their extremities (Yu et al., 2020). In the case of the PR-B homodimer structure, the monomer NTDs neither mask AF2 nor make direct contact with each other. The net result of this spatial configuration is that the PR-B can avail three AFs for coactivator recruitment whereas AR depends heavily on one. Therefore, the PR-B complex structure reinforces our original finding that dimeric NRs co-opt different topologies and spatial arrangements on DNA, despite their similar functional domain organizations (Yi et al., 2021). Such structural differences predict that subsequent coactivator assembly mechanisms also will be markedly different, leading to core transcriptional complexes with significantly distinct quaternary structures.

The core PR-B transcriptional complex comprises the PR-B dimer assembled with one SRC-2 and one p300. The stoichiometry of the PR-B core transcriptional complex significantly differs from the corresponding ERα complex, which instead recruits two primary coactivators and one p300 (Yi et al., 2015). As predicted from our PR-B dimer structure above, both AF3s directly contact p300 in the PR-B core transcriptional complex. However, only the PR-B LBD-a directly contacts p300, suggesting that LBD-b is free to interact with other coactivators as the core transcriptional complex further nucleates prior to initiation of transcription (O'Malley, 2003). Based on C-Fab recognition of the region adjacent to AF2, we found that PR-B AF2 and AF3 are involved in binding p300 (Figure S2D). Mutation of the key residue in this region (E911A) inhibits PR transcriptional activity (Gong et al., 1997; Wen et al., 1994). Unlike PR-B and AR (Yu et al., 2020), the ERα dimer does not directly contact p300 but instead uses two SRCs to indirectly enlist p300, which indicates that absence of a large multi-domain NTD in ERα necessitates the recruitment of an additional primary SRC to bridge the gap between the NR and a secondary coactivator. The AF2 of ERα is required for interacting with SRCs (Feng et al., 1998; Shiau et al., 1998; Yi et al., 2015) instead of p300 as observed in the PR-B

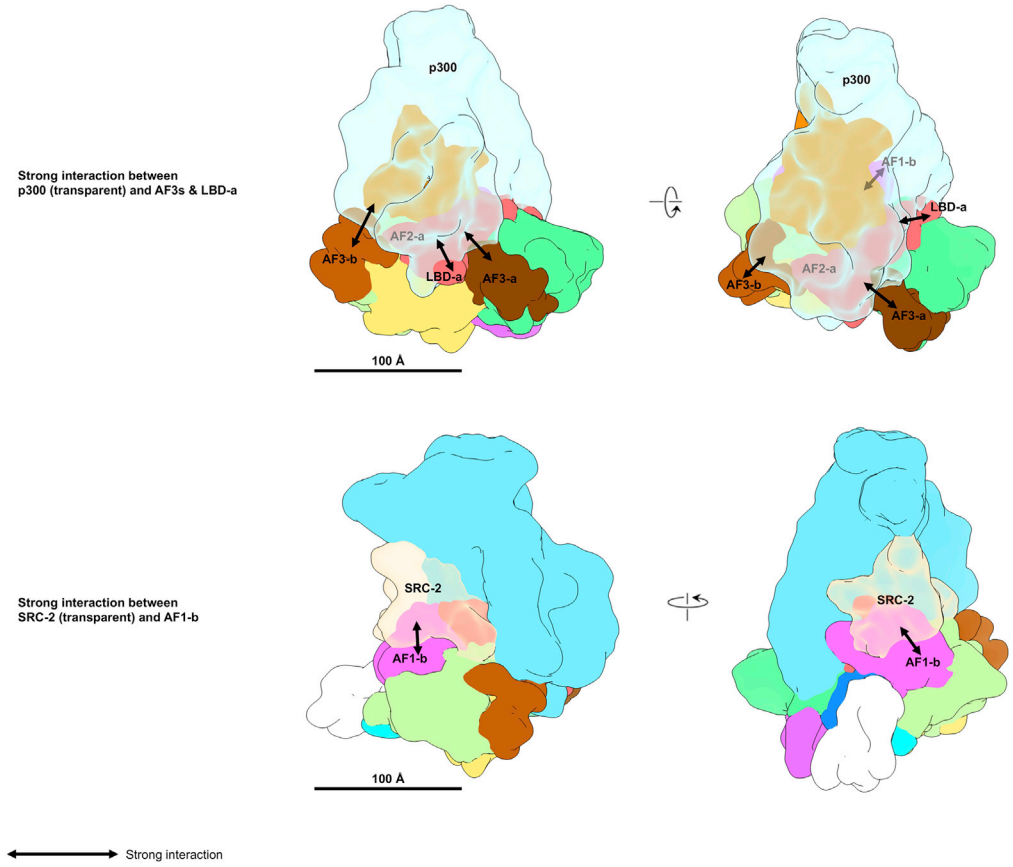


**Figure 5. Model of full-length PR-B domain organization and the contribution of each AF in SRC-2 and p300 coactivator recruitment**

Shown is the illustration of the assembled PRE-DNA/PR/SRC-2/p300 structure demonstrating the strong interaction between p300 (transparent) and two AF3s & LBD-a (AF2-a) (top panel), and the strong interaction between SRC-2 (transparent) and AF1-b (bottom panel). See also Figure S5. The scale bars represent 100 angstrom.

complex. Although the AR directly contacts p300 within its core transcriptional complex, direct contact is made exclusively through its N-terminal AF1 (Yu et al., 2020). Within the PR-B core transcriptional complex, a single SRC-2 molecule is wedged between the PR-B dimers and p300. The AF1-b in the PR-B's NTD-b region forms a key interface between PR-B and SRC-2. While this observation agrees with our biochemical data here and previous studies elsewhere (Goswami et al., 2014; Kumar et al., 2013; Onate et al., 1998; Woo et al., 2019) that support a pivotal role for AF1 in primary coactivator recruitment, these findings underscore a "division of labor" between the PR-B monomers when it comes to both primary and secondary coactivator recruitment during formation of the core transcriptional complex.

The quaternary structures for the PR-B dimeric and core transcriptional complexes on DNA now provide the pretext for similar structural studies on the PR-A isoform in the future. Structures of each isoform complex will be required to delineate the structural similarities and differences to explain their common and divergent transactivational responses to progesterone ligand shown *in vitro* and *in vivo* (Jacobsen and Horwitz, 2012). Our structural analysis underscores a pivotal role for the PR-B-specific AF3 region as a direct contact with the secondary p300 coactivator, suggesting that the absence of AF3 in the PR-A isoform will block direct secondary coactivator contact. We also predict that without the AF3, the tertiary conformation of PR-A will markedly differ from PR-B, resulting in isoform-specific differences in intramolecular interdomain allosteric crosstalk within their respective transcriptional complexes.

Apart from elucidating the fundamental structural differences of the core transcriptional complexes that underpin the distinct transactivational properties of each member of the NR triad that is responsible for

**Table 1. Comparison of three steroid receptor dimer structures and the complex assembly mechanisms with coactivators**

ERα, AR, PR-B complexes comparison

| | ERα | AR | PR-B |
|---|---|---|---|
| Dimer 2-fold symmetric structure | Yes | No | Yes |
| LBDs at the center of dimer interface | Yes | Yes | Yes |
| NTD-LBD spatial organization | Each NTD is at one side of LBD | The NTD wraps around the LBD | Each NTD is at one side of LBD |
| Coactivator binding | Two SRC-3<br>One p300 | One SRC-3<br>One p300 | One SRC-2<br>One p300 |
| Receptor-SRC contact site | Mainly LBD (AF2) | N-terminal end close to the FXXLF motif | AF1 close to the DBD |
| Receptor-p300 direct interaction | No | Yes (AF1) | Yes (AF3, AF2 and AF1) |

See also Figures S2–S5 and Table S1.

mediating sex steroid hormone action in reproduction, the PR-B structures—their protein-protein interaction regions in particular—may offer a paradigm shift in rational drug design that takes into account the intact receptor complexed with full-length coactivators rather than just focusing on one domain. Following a holistic-based structure-based design framework would significantly expand the options for progestin therapy currently available to treat a spectrum of gynecological disorders, from uterine fibroids to endometriosis (Critchley and Chodankar, 2020; Vannuccini et al., 2021).

## Limitations of the study

In this study, we identified the contributions of each AF and demonstrate their structural basis in forming the PR-B dimer interface and PR-B/coactivator complex. Based on the structural information, we proposed a mechanism of how each of the protein components contact with the other two proteins within the complex to form a core functional active transcription unit. Nevertheless, there are limitations of structural resolution associated with the endogenous flexibility of each component. The PR-B structure was roughly segmented into regions based on Segger in Chimera with watershed algorithm and validated by antibodies recognition. The atomic-level structural details like side chain orientations or exact boundaries of regions are missing. Thus, the deficiency of atomic structure details for interface residues leads to limitation for further discussion of interactions between PR-B and its coactivators. Besides, the structures of another functional isoform PR-A without the AF3 remain unknown. PR-A will obviously differ from PR-B, resulting in isoform-specific differences in intramolecular interdomain allosteric crosstalk within their respective transcriptional complexes. However, all the differences of PR-A and PR-B were indirectly analyzed based on known structures for the PR-B. Further structural investigation of PR-A is needed.

## STAR★METHODS

Detailed methods are provided in the online version of this paper and include the following:

- KEY RESOURCES TABLE
- RESOURCE AVAILABILITY
  - Lead contact
  - Materials availability
  - Data and code availablility
- EXPERIMENTAL MODEL AND SUBJECT DETAILS
  - Cell culture
- METHOD DETAILS
  - Protein expression and purification
  - GST pull-down experiment
  - *In vitro* transcription
  - Immunodepletion
  - Cryo-EM specimen preparation and data collection

- Cryo-EM data processing
- Antibody labeling and structure segmentation with interaction validation

- QUANTIFICATION AND STATISTICAL ANALYSIS

## SUPPLEMENTAL INFORMATION

Supplemental information can be found online at https://doi.org/10.1016/j.isci.2022.105321.

## ACKNOWLEDGMENTS

We thank Dr. Dean Edwards at Baylor College of Medicine for providing the PR-B expressing baculovirus. This work is supported by NIH (R01 HD008188, HD007857, and NIDDK59820) to B.W.O.; Robert Welch Foundation (Q-1967-20180324), NIH-GMS (R01 GM143380), and BCM BMB department seed funds to Z.W.; DOD (DAMD W81WH-21-1-0404) to P.Y.; NIH/NICHD R01 HD042311 to J.P.L.; NIH (R01GM080139) to S.L.; and NCI Cancer CenterSupport Grant P30CA125123 (Proteomic Shared Resource of Dan L Duncan Comprehensive Cancer Center). The Monoclonal Antibody and Protein Production Core is an Advanced Technology Core supported by BCM. Data were collected using instrumentation purchased under CPRIT RP190602 as part of the CryoEM Advanced Technical Core at Baylor College of Medicine, cryo-EM core at UTHealth Center at Houston, and National Cancer Institute's National Cryo-EM Facility (NCEF).

## AUTHOR CONTRIBUTIONS

P.Y., Z.W., and B.W.O. conceived and designed the experiments. X.Y., Z.W., and S.J.L. did cryo-EM imaging and computational analysis. P.Y. and L.E.V.L. performed the biochemical experiments. A.K.P. performed *in vitro* transcription assay. P.Y., X.Y., J.P.L., D.M.L., Z.W., S.J.L., and B.W.O. interpreted the data and wrote the manuscript. All authors discussed the results and commented on the manuscript.

## DECLARATION OF INTERESTS

The authors declare no competing interests.

Received: April 25, 2022
Revised: June 27, 2022
Accepted: October 7, 2022
Published: November 18, 2022

## REFERENCES

Bell, J.M., Chen, M., Baldwin, P.R., and Ludtke, S.J. (2016). High resolution single particle refinement in EMAN2.1. Methods *100*, 25–34.

Critchley, H.O.D., and Chodankar, R.R. (2020). 90 years of progesterone: selective progesterone receptor modulators in gynaecological therapies. J. Mol. Endocrinol. *65*, T15–T33.

Danielian, P.S., White, R., Lees, J.A., and Parker, M.G. (1992). Identification of a conserved region required for hormone dependent transcriptional activation by steroid hormone receptors. EMBO J. *11*, 1025–1033.

DeMayo, F.J., and Lydon, J.P. (2020). 90 years of progesterone: new insights into progesterone receptor signaling in the endometrium required for embryo implantation. J. Mol. Endocrinol. *65*, T1–T14.

Diep, C.H., Daniel, A.R., Mauro, L.J., Knutson, T.P., and Lange, C.A. (2015). Progesterone action in breast, uterine, and ovarian cancers. J. Mol. Endocrinol. *54*, R31–R53.

Dong, X., Challis, J.R.G., and Lye, S.J. (2004). Intramolecular interactions between the AF3 domain and the C-terminus of the human progesterone receptor are mediated through two LXXLL motifs. J. Mol. Endocrinol. *32*, 843–857.

Dubochet, J., Adrian, M., Chang, J.J., Homo, J.C., Lepault, J., McDowall, A.W., and Schultz, P. (1988). Cryo-electron microscopy of vitrified specimens. Q. Rev. Biophys. *21*, 129–228.

Feng, W., Ribeiro, R.C., Wagner, R.L., Nguyen, H., Apriletti, J.W., Fletterick, R.J., Baxter, J.D., Kushner, P.J., and West, B.L. (1998). Hormone-dependent coactivator binding to a hydrophobic cleft on nuclear receptors. Science *280*, 1747–1749.

Gong, W., Chávez, S., and Beato, M. (1997). Point mutation in the ligand-binding domain of the progesterone receptor generates a transdominant negative phenotype. Mol. Endocrinol. *11*, 1476–1485.

Goswami, D., Callaway, C., Pascal, B.D., Kumar, R., Edwards, D.P., and Griffin, P.R. (2014). Influence of domain interactions on conformational mobility of the progesterone receptor detected by hydrogen/deuterium exchange mass spectrometry. Structure *22*, 961–973.

Grimm, S.L., Hartig, S.M., and Edwards, D.P. (2016). Progesterone receptor signaling mechanisms. J. Mol. Biol. *428*, 3831–3849.

Guo, H., Franken, E., Deng, Y., Benlekbir, S., Singla Lezcano, G., Janssen, B., Yu, L., Ripstein, Z.A., Tan, Y.Z., and Rubinstein, J.L. (2020). Electron-event representation data enable efficient cryoEM file storage with full preservation of spatial and temporal resolution. IUCrJ *7*, 860–869.

Henderson, R., Sali, A., Baker, M.L., Carragher, B., Devkota, B., Downing, K.H., Egelman, E.H., Feng, Z., Frank, J., Grigorieff, N., et al. (2012). Outcome of the first electron microscopy validation task force meeting. Structure *20*, 205–214.

Hill, K.K., Roemer, S.C., Churchill, M.E.A., and Edwards, D.P. (2012). Structural and functional analysis of domains of the progesterone receptor. Mol. Cell. Endocrinol. *348*, 418–429.

Horwitz, K.B., and Sartorius, C.A. (2020). 90 years of progesterone: progesterone and progesterone receptors in breast cancer: past, present, future. J. Mol. Endocrinol. *65*, T49–T63.

Ishikawa, H., Ishi, K., Serna, V.A., Kakazu, R., Bulun, S.E., and Kurita, T. (2010). Progesterone is essential for maintenance and growth of uterine leiomyoma. Endocrinology *151*, 2433–2442.

Jacobsen, B.M., and Horwitz, K.B. (2012). Progesterone receptors, their isoforms and progesterone regulated transcription. Mol. Cell. Endocrinol. *357*, 18–29.

Kamei, Y., Xu, L., Heinzel, T., Torchia, J., Kurokawa, R., Gloss, B., Lin, S.C., Heyman, R.A., Rose, D.W., Glass, C.K., and Rosenfeld, M.G. (1996). A CBP integrator complex mediates transcriptional activation and AP-1 inhibition by nuclear receptors. Cell *85*, 403–414.

Kim, O., Park, E.Y., Kwon, S.Y., Shin, S., Emerson, R.E., Shin, Y.H., DeMayo, F.J., Lydon, J.P., Coffey, D.M., Hawkins, S.M., et al. (2020). Targeting progesterone signaling prevents metastatic ovarian cancer. Proc. Natl. Acad. Sci. USA *117*, 31993–32004.

Kommagani, R., Szwarc, M.M., Kovanci, E., Creighton, C.J., O'Malley, B.W., Demayo, F.J., and Lydon, J.P. (2014). A murine uterine transcriptome, responsive to steroid receptor coactivator-2, reveals transcription factor 23 as essential for decidualization of human endometrial stromal cells. Biol. Reprod. *90*, 75.

Kommagani, R., Szwarc, M.M., Kovanci, E., Gibbons, W.E., Putluri, N., Maity, S., Creighton, C.J., Sreekumar, A., DeMayo, F.J., Lydon, J.P., and O'Malley, B.W. (2013). Acceleration of the glycolytic flux by steroid receptor coactivator-2 is essential for endometrial decidualization. PLoS Genet. *9*, e1003900.

Kumar, R., Moure, C.M., Khan, S.H., Callaway, C., Grimm, S.L., Goswami, D., Griffin, P.R., and Edwards, D.P. (2013). Regulation of the structurally dynamic N-terminal domain of progesterone receptor by protein-induced folding. J. Biol. Chem. *288*, 30285–30299.

Meyer, M.E., Pornon, A., Ji, J.W., Bocquel, M.T., Chambon, P., and Gronemeyer, H. (1990). Agonistic and antagonistic activities of RU486 on the functions of the human progesterone receptor. EMBO J. *9*, 3923–3932.

Mukherjee, A., Soyal, S.M., Fernandez-Valdivia, R., Gehin, M., Chambon, P., Demayo, F.J., Lydon, J.P., and O'Malley, B.W. (2006). Steroid receptor coactivator 2 is critical for progesterone-dependent uterine function and mammary morphogenesis in the mouse. Mol. Cell Biol. *26*, 6571–6583.

O'Malley, B.W. (2003). Sequentiality and processivity of nuclear receptor coregulators in regulation of target gene expression. Nucl. Recept. Signal. *1*, e010.

O'Malley, B.W. (2020). 90 years of progesterone: Reminiscing on the origins of the field of progesterone and estrogen receptor action. J. Mol. Endocrinol. *65*, C1–C4.

Onate, S.A., Boonyaratanakornkit, V., Spencer, T.E., Tsai, S.Y., Tsai, M.J., Edwards, D.P., and O'Malley, B.W. (1998). The steroid receptor coactivator-1 contains multiple receptor interacting and activation domains that cooperatively enhance the activation function 1 (AF1) and AF2 domains of steroid receptors. J. Biol. Chem. *273*, 12101–12108.

Panigrahi, A.K., Foulds, C.E., Lanz, R.B., Hamilton, R.A., Yi, P., Lonard, D.M., Tsai, M.J., Tsai, S.Y., and O'Malley, B.W. (2018). SRC-3 coactivator governs dynamic estrogen-induced chromatin looping interactions during transcription. Mol. Cell *70*, 679–694.e7.

Patel, B., Elguero, S., Thakore, S., Dahoud, W., Bedaiwy, M., and Mesiano, S. (2015). Role of nuclear progesterone receptor isoforms in uterine pathophysiology. Hum. Reprod. Update *21*, 155–173.

Pintilie, G., and Chiu, W. (2012). Comparison of Segger and other methods for segmentation and rigid-body docking of molecular components in cryo-EM density maps. Biopolymers *97*, 742–760.

Punjani, A., Rubinstein, J.L., Fleet, D.J., and Brubaker, M.A. (2017). cryoSPARC: algorithms for rapid unsupervised cryo-EM structure determination. Nat. Methods *14*, 290–296.

Rohou, A., and Grigorieff, N. (2015). CTFFIND4: fast and accurate defocus estimation from electron micrographs. J. Struct. Biol. *192*, 216–221.

Sartorius, C.A., Melville, M.Y., Hovland, A.R., Tung, L., Takimoto, G.S., and Horwitz, K.B. (1994). A third transactivation function (AF3) of human progesterone receptors located in the unique N-terminal segment of the B-isoform. Mol. Endocrinol. *8*, 1347–1360.

Scheres, S.H.W. (2012). RELION: implementation of a Bayesian approach to cryo-EM structure determination. J. Struct. Biol. *180*, 519–530.

Shiau, A.K., Barstad, D., Loria, P.M., Cheng, L., Kushner, P.J., Agard, D.A., and Greene, G.L. (1998). The structural basis of estrogen receptor/coactivator recognition and the antagonism of this interaction by tamoxifen. Cell *95*, 927–937.

Takimoto, G.S., Tung, L., Abdel-Hafiz, H., Abel, M.G., Sartorius, C.A., Richer, J.K., Jacobsen, B.M., Bain, D.L., and Horwitz, K.B. (2003). Functional properties of the N-terminal region of progesterone receptors and their mechanistic relationship to structure. J. Steroid Biochem. Mol. Biol. *85*, 209–219.

Tang, G., Peng, L., Baldwin, P.R., Mann, D.S., Jiang, W., Rees, I., and Ludtke, S.J. (2007). EMAN2: an extensible image processing suite for electron microscopy. J. Struct. Biol. *157*, 38–46.

Tetel, M.J., Giangrande, P.H., Leonhardt, S.A., McDonnell, D.P., and Edwards, D.P. (1999). Hormone-dependent interaction between the amino- and carboxyl-terminal domains of progesterone receptor *in vitro* and *in vivo*. Mol. Endocrinol. *13*, 910–924.

Tsai, M.J., and O'Malley, B.W. (1994). Molecular mechanisms of action of steroid/thyroid receptor superfamily members. Annu. Rev. Biochem. *63*, 451–486.

Tung, L., Abdel-Hafiz, H., Shen, T., Harvell, D.M.E., Nitao, L.K., Richer, J.K., Sartorius, C.A., Takimoto, G.S., and Horwitz, K.B. (2006). Progesterone receptors (PR)-B and -A regulate transcription by different mechanisms: AF-3 exerts regulatory control over coactivator binding to PR-B. Mol. Endocrinol. *20*, 2656–2670.

Tung, L., Shen, T., Abel, M.G., Powell, R.L., Takimoto, G.S., Sartorius, C.A., and Horwitz, K.B. (2001). Mapping the unique activation function 3 in the progesterone B-receptor upstream segment. Two LXXLL motifs and a tryptophan residue are required for activity. J. Biol. Chem. *276*, 39843–39851.

Vannuccini, S., Clemenza, S., Rossi, M., and Petraglia, F. (2021). Hormonal treatments for endometriosis: the endocrine background. Rev. Endocr. Metab. Disord. *23*, 333–355.

Wang, Z., Hryc, C.F., Bammes, B., Afonine, P.V., Jakana, J., Chen, D.H., Liu, X., Baker, M.L., Kao, C., Ludtke, S.J., et al. (2014). An atomic model of brome mosaic virus using direct electron detection and real-space optimization. Nat. Commun. *5*, 4808.

Wardell, S.E., Kwok, S.C., Sherman, L., Hodges, R.S., and Edwards, D.P. (2005). Regulation of the amino-terminal transcription activation domain of progesterone receptor by a cofactor-induced protein folding mechanism. Mol. Cell Biol. *25*, 8792–8808.

Wen, D.X., Xu, Y.F., Mais, D.E., Goldman, M.E., and McDonnell, D.P. (1994). The A and B isoforms of the human progesterone receptor operate through distinct signaling pathways within target cells. Mol. Cell Biol. *14*, 8356–8364.

Williams, S.P., and Sigler, P.B. (1998). Atomic structure of progesterone complexed with its receptor. Nature *393*, 392–396.

Woo, A.R.E., Sze, S.K., Chung, H.H., and Lin, V.C.L. (2019). Delineation of critical amino acids in activation function 1 of progesterone receptor for recruitment of transcription coregulators. Biochim. Biophys. Acta. Gene Regul. Mech. *1862*, 522–533.

Yi, P., Wang, Z., Feng, Q., Chou, C.K., Pintilie, G.D., Shen, H., Foulds, C.E., Fan, G., Serysheva, I., Ludtke, S.J., et al. (2017). Structural and functional impacts of ER coactivator sequential recruitment. Mol. Cell *67*, 733–743.e4.

Yi, P., Wang, Z., Feng, Q., Pintilie, G.D., Foulds, C.E., Lanz, R.B., Ludtke, S.J., Schmid, M.F., Chiu, W., and O'Malley, B.W. (2015). Structure of a biologically active estrogen receptor-coactivator complex on DNA. Mol. Cell *57*, 1047–1058.

Yi, P., Yu, X., Wang, Z., and O'Malley, B.W. (2021). Steroid receptor-coregulator transcriptional complexes: new insights from CryoEM. Essays Biochem. *65*, 857–866.

Yu, X., Yi, P., Hamilton, R.A., Shen, H., Chen, M., Foulds, C.E., Mancini, M.A., Ludtke, S.J., Wang, Z., and O'Malley, B.W. (2020). Structural insights of transcriptionally active, full-length Androgen receptor coactivator complexes. Mol. Cell *79*, 812–823.e4.

Zheng, S.Q., Palovcak, E., Armache, J.P., Verba, K.A., Cheng, Y., and Agard, D.A. (2017). MotionCor2: anisotropic correction of beam-induced motion for improved cryo-electron microscopy. Nat. Methods *14*, 331–332.

## STAR★METHODS

### KEY RESOURCES TABLE

| REAGENT or RESOURCE | SOURCE | IDENTIFIER |
|---|---|---|
| Antibodies | | |
| PRB-N Ab | Santa Cruz | Cat#Sc-811; RRID:AB_628173 |
| PRB-C-Ab | Santa Cruz | Cat# sc-53943; RRID:AB_831674 |
| HA Ab | Santa Cruz | Cat# sc-805, RRID:AB_631618 |
| Flag M2 beads | Sigma | Cat#F2426; RRID:AB_2616449 |
| P300 | Santa Cruz | Cat#Sc-584; RRID:AB_2293429 |
| Flag-HRP | Sigma | Cat#A8592; RRID:AB_439702 |
| Bacterial and virus strains | | |
| *E.coli* BL21 (DE3) | Agilent | Cat#200131 |
| Chemicals, peptides, and recombinant proteins | | |
| SRC-2 | Monoclonal Antibody/Recombinant Protein Expression Core at BCM | N/A |
| P300 | Monoclonal Antibody/Recombinant Protein Expression Core at BCM | N/A |
| PR-B | Monoclonal Antibody/Recombinant Protein Expression Core at BCM | N/A |
| Dynabeads™ M-280 Streptavidin | Thermo Fisher | Cat#11205D |
| Progesterone | Sigma | Cat#P0130 |
| Glutathione Sepharose 4B | GE Life Sciences | Cat#17075601 |
| Pierce Fab MicroPreparation Kit | Thermo Fisher | Cat#44685 |
| Deposited data | | |
| CryoEM maps of PRE-DNA/PR-B | This study | EMDB: EMD-27537 |
| CryoEM maps of PRE-DNA/PR-B/SRC-2/p300 | This study | EMDB: EMD-27540 |
| CryoEM maps of PRE-DNA/PR-B/N-Fab | This study | EMDB: EMD-27537 |
| CryoEM maps of PRE-DNA/PR-B/C-Fab | This study | EMDB: EMD-27537 |
| CryoEM maps of PRE-DNA/PR-B/SRC-2/p300/N-Fab | This study | EMDB: EMD-27540 |
| Experimental models: Cell lines | | |
| HEK 293T/17 | Tissue Culture Core (BCM) | Cat#ATCC® CRL-11268™ |
| Sf9 | Monoclonal Antibody/recombinant Protein Expression Core (BCM) | Cat# ATCC® CRL-1711™ |
| Oligonucleotides | | |
| PRE PCR forward primer | Thermo Fisher | N/A |
| PRE PCR reverse primer | Thermo Fisher | N/A |
| ARE/PRE oligonucleotide | Santa Cruz | Cat#sc-2551 |
| Recombinant DNA | | |
| pSG5-HA-PRB | This study | N/A |
| pCMV-flag-SRC-3 WT/Mut | This study | N/A |
| pGEX-SRC-2 fragments | This study | N/A |

(*Continued on next page*)

*Continued*

| REAGENT or RESOURCE | SOURCE | IDENTIFIER |
|---|---|---|
| 3XARE/PRE-E4 | Yu et al.,2020 | N/A |
| Software and algorithms | | |
| EMAN2.3 | https://cryoem.bcm.edu/cryoem/downloads/view_eman2_versions | N/A |
| Relion3.1 | https://www3.mrc-lmb.cam.ac.uk/relion/index.php/Download_%26_install | N/A |
| *Gctf* | https://www2.mrc-lmb.cam.ac.uk/research/locally-developed-software/zhang-software/ | N/A |
| Chimera | https://www.cgl.ucsf.edu/chimera/download.html | N/A |
| ChimeraX | https://www.rbvi.ucsf.edu/chimerax/download.html | N/A |
| Other | | |
| SerialEM | http://bio3d.colorado.edu/SerialEM/ | N/A |

## RESOURCE AVAILABILITY

### Lead contact

Requests for reagents and further information should be directed to the lead contact, Bert W O'Malley (berto@bcm.edu).

### Materials availability

This study did not generate new unique reagents. Plasmids generated in this study will be available upon request.

### Data and code availablility

All generated maps and models have been deposited to EMDataBank and are publicly available as of the date of publication. IDs are listed in the key resources table and Table S1. This paper does not report original code. Any additional information required to reanalyze the data reported in this paper is available from the lead contact upon request.

## EXPERIMENTAL MODEL AND SUBJECT DETAILS

### Cell culture

Sf9 insect cell line is a clonal isolate of *Spodoptera frugiperda* Sf21 cells (IPLB-Sf21-AE). Sf9 cells were cultured in ESF 921 Insect Cell Culture Medium.

## METHOD DETAILS

### Protein expression and purification

The protein purification methods are similar as the methods we published previously (Yi et al., 2015; Yu et al., 2020). Sf9 insect cells were infected with His-PR-B expressing baculoviruses (that were produced in BCM Monoclonal Antibody/recombinant Protein Expression Core Facility). Cells were harvested 48 hours post-infection. Cells were washed and spined down at 5,000 rpm for 10 min at 4°C. Sf9 cells were further resuspended in a lysis buffer (50 mM Tris-HCl, pH 8.0; 150 mM NaCl; 100 nM progesterone; 0.5% NP40) and lysed using a homogenizer. After 40 min centrifugation at 15,000 rpm, the cleared lysate was incubated with Ni-NTA (Qiagen) resins, washed three times with wash buffer (50 mM Tris-HCl, pH8.0; 150 mM NaCl; 100 nM R1881; 0.05% NP40; 25 mM imidazole) and finally eluted with elution buffer (50 mM Tris-HCl, pH8.0; 150 mM NaCl; 100 nM progesterone; 0.05% NP40; 300 mM imidazole). Eluted protein was further applied on a gel-filtration column (Superdex 200 Increase 10/300 GL, GE Healthcare) pre-equilibrated with gel filtration buffer (50 mM Tris-HCl, pH8.0; 150 mM NaCl; 100 nM progesterone; 0.05% NP40). Purified protein fractions were pooled together (~0.5 mg/mL) and for all the studies.

Baculovirus-expressing His- and flag-tagged human recombinant SRC-2 purified through Nickel affinity purification followed by flag affinity purification. His-tagged human recombinant p300 protein was expressed in baculoviruses and purified through Nickel affinity purification. GST-fused SRC-2 fragments were expressed in E.coli and purified using glutathione sepharose beads.

### GST pull-down experiment

The methods are similar as the methods we published previously (Yi et al., 2015; Yu et al., 2020). Different PR-B or SRC-2 fragments were fused to GST in a pGEX-4T1 vector and the proteins were expressed in *E.coli*. Bacterial lysates containing expressed different GST-fused proteins were incubated with 6 ul of glutathione sepharose 4B beads (GE Healthcare Life Sciences) for 1 hour and then washed 3 times with wash buffer (20mM HEPES pH 7.6, 150mM KCl, 1mM DTT, 0.1% NP40, 8% glycerol and protease inhibitor cocktail). The beads were then incubated with full-length recombinant proteins purified from baculovirus (SRC-2, p300 for GST-PR-B; PR-B, p300 for GST-SRC-2) for 3 hours. After extensive wash, the beads were boiled in a 2x SDS sample buffer and then loaded to a 4–15% SDS-PAGE.

### *In vitro* transcription

Chromatin reconstitution and *in vitro* transcription (IVT) of the GREB1 composite fragment (CompF) was performed as described (Panigrahi et al., 2018). Briefly, each IVT reaction contained 0.2 pmoles of chromatinized templates and 10-fold molar excess of recombinant PR-B, and 50 μg of HeLa nuclear extracts (control as well as SRC-2/p300 immunodepleted) were used in each IVT reaction as indicated. Two pmoles of purified recombinant SRC-2 and p300 were used as indicated. After 50 min of IVT reaction, RNA was extracted with TriReagent, digested with Turbo-DNA-free DNase kit (Invitrogen AM1907), and analyzed by 1-step RT-qPCR using primers specific for GREB1 mRNA (Panigrahi et al., 2018).

### Immunodepletion

Immunodepletion was essentially performed as detailed (Panigrahi et al., 2018). One mg of HeLa NE was immunodepleted with control rabbit + mouse IgG (EMD-Millipore 12–370 and 12–371, respectively; 5 μg each) or antibodies against SRC-2 (Cell Signaling #96687) and p300 (Santa Cruz sc-48343), 5 μg each.

### Cryo-EM specimen preparation and data collection

For the structure of DNA-bound PR, purified His-tagged PR was incubated with a 32 bp PRE/ARE-consensus oligo (Santa Cruz, sc-2551) in the presence of 1 μM progesterone. For the structure of DNA-bound PR-B/SRC-2/p300 complex, a 324 bp long biotinylated PRE/ARE-containing DNA was used (Yu et al., 2020). 0.6 μg of recombinant PR-B, SRC-2 and p300 proteins were incubated with 200 ng of PREDNA in the presence of 1 μM progesterone on ice for 1 hour. The mixture was then incubated with 15 μL Dynabeads M280 streptavidin (Invitrogen) for 15 min at room temperature followed by restriction enzyme digestion to release the DNA-bound protein complex from the beads. The sample was kept on ice before vitrification (Dubochet et al., 1988) on the grid. A 3.5 μL sample was applied onto a 200-mesh R1.2/1.3 Quantifoil holy carbon grid covered with graphene oxide (GO)-coated grid following the same preparation pipeline (Yu et al., 2020). After applying the sample, the grid was blotted and rapidly frozen in liquid ethane using a Vitrobot IV (FEI), with constant temperature and humidity during the process of blotting. The grid was stored in liquid nitrogen before imaging.

7,011 movie stacks for PRE-DNA/PR-B were collected at 200 kV on the Falcon 4 Electron Detector on the Glacios™ Cryo-TEM (Thermo Fisher). Images of PRE-DNA/PR-B were collected in dose fractionation super-resolution counting mode at 150,000x magnification, corresponding to a calibrated physical pixel size of 0.968 Å, with a defocus range from −1.0 to −2.6 μm. The total exposure time for the dataset was 8s, leading to a total accumulated dose of 55 electrons*$Å^{-2}$ on the specimen. Each image stack was fractionated into 40 subframes, each with an accumulation time of 0.2 s per frame.

1,201 movie stacks for PRE-DNA/PR-B/SRC-2/p300 complex at 300 kV on K2 summit on the NCEF Titan Krios. Images of PRE-DNA/PR-B/SRC-2/p300 complex were collected in dose fractionation super-resolution counting mode at 105,000x magnification, corresponding to a calibrated physical pixel size of 1.32 Å, with a defocus range from −1.0 to −2.5 mm. The total exposure time for the dataset was 10 s, leading to a total accumulated dose of 50 electrons*$Å^{-2}$ on the specimen. Each image stack was fractionated into 50 subframes, each with an accumulation time of 0.2 s per frame.

Following the same procedure with PRE-DNA/PR-B, grids of the PRE-DNA/PR-B sample with N-Fab or C-Fab and PRE-DNA/PR-B/SRC-2/p300 sample with N-Fab were prepared. The images of these four samples were taken in the same procedure as PRE-DNA/PR-B mentioned above. The total image numbers of these three samples are shown in Table S1.

### Cryo-EM data processing

The final frame average of PRE-DNA/PR-B and PRE-DNA/PR-B/SRC-2/p300 were computed from averages of every three consecutive frames to correct beam-induced motion correction during exposure by MotionCor2 (Zheng et al., 2017) CTF parameters of the particles in each frame average was determined by program *e2ctf.py* in EMAN2 (Tang et al., 2007) and CTFFIND (Rohou and Grigorieff, 2015). A total of 341,819 particles images for PRE-DNA/PR-B and 194,158 particles images for PRE-DNA/PR-B/SRC-2/p300 were automatically boxed out by newly developed e2boxer.py in EMAN2 (Bell et al., 2016) with a box size of 280 × 280 pixels using the averaged sum of 40 and 50 raw frames (representative) per specimen area. The particle intensity in each frame was weighted according to a radiation damage model (Guo et al., 2020; Wang et al., 2014; Zheng et al., 2017) (courtesy of B. Bammes of Direct Electron, LP). 2D reference free class averages were computed by RELION 3.1 (Scheres, 2012). Initial models for every reconstruction were generated from scratch by *e2initialmodel.py* program using selected good quality 2D averages based on the 2D averages results. Refinements were carried out by RELION 3.1 and cryoSPARC, low pass filtered to 60Å, with search angle of 7.5 degrees for 11 iterations and subsequently with an angular sampling of 0.9375 degrees for 14 iterations. 42,619 particles images for PRE-DNA/PR-B and 15,779 particles images for PRE-DNA/PR-B/SRC-2/p300 were applied to final reconstruction yielding a resolution of 10.9 Å and 19.1 Å, respectively, at 0.143 of the Fourier shell correlation (FSC). The PR-B binds to the PREDNA at the center of the complex density. During refinement and classification, approximately 60% of particles were observed without bound DNA, which were excluded from the final refinement, but the DNA density is still somewhat weaker than expected due to particle classification accuracy in ice.

Following the same procedure, other antibody related structures were carried out. The particle numbers and final resolution are shown in Table S1.

### Antibody labeling and structure segmentation with interaction validation

Full segmentation of the complex followed the same protocol as ERα complex and AR complex using Segger in Chimera with watershed algorithm (Pintilie and Chiu, 2012). Regions of each segment were identified by specific antibody labeling first. The ratio between each segmented component volume is consistent with the ratio of corresponding domain masses. The boundary of PRE-DNA/PR-B segmented domains was determined according to the rigid body docking result of LBD crystal structures and the relative ratios of each domain. The boundary between each component in the PRE-DNA/PR-B/SRC-2/p300 complex was refined based on the previous knowledge of PR-B, p300 and SRC-2. The ratio between each component was validated by the molecular weight ratio as described in the previous ERα and AR structures (Yi et al., 2015; Yu et al., 2020).

## QUANTIFICATION AND STATISTICAL ANALYSIS

The quantification and statistical analyses are integral parts of the software and algorithms used. Details are described in the main text and STAR Methods sections.